Journal of Organometallic Chemistry 892 (2019) 83–88

Contents lists available at ScienceDirect

Journal of Organometallic Chemistry

journal homepage: www.elsevier.com/locate/jorganchem

Amphiphilic bimetallic polymer as single-source precursors for the one-pot synthesis of $L1_0$-phase FePt nanoparticles

Zhengong Meng [a], Zhuoxun Wei [a], Kuo Fu [a], Lei Lv [a], Zhen-Qiang Yu [a, *], Wai-Yeung Wong [b, **]

[a] College of Chemistry and Environmental Engineering, Shenzhen University, Shenzhen, Guangdong, China
[b] Department of Applied Biology and Chemical Technology, The Hong Kong Polytechnic University, Hung Hom, Hong Kong, China

ARTICLE INFO

Article history:
Received 29 March 2019
Received in revised form
16 April 2019
Accepted 18 April 2019
Available online 20 April 2019

Keywords:
FePt nanoparticles
Amphiphilic polymer
Single-source precursor
Size effect
Self-assembly

ABSTRACT

Amphiphilic polymers have attracted extensive research attention in constructing various nanostructures by self-assembly. Here we designed and synthesized two amphiphilic bimetallic polymers with different length of the tails **P1** and **P2**, in which Fe,Pt-containing conjugated complex acted as the hydrophobic block and hydrophilic poly(ethylene glycol) (PEG) was bonded to the bimetallic core as the flexible tails. **P1** and **P2** were used as the single-source precursors to prepare FePt nanoparticles (NPs) by one-pot pyrolysis. The resultant NPs were fully characterized and had a chemically ordered face-centered tetragonal (fct) phase with high crystallinity. The size of NPs pyrolyzed from **P1** and **P2** was 24.7 and 8.2 nm with the relative coercivity of 9.6 and 1.3 kOe, respectively. The difference was preliminarily explained by the discrepancy of their degrees of crystallinity, and also analyzed by the precursors' structural effect. The amphiphilic design showed a good potential in preparing monodisperse ferromagnetic FePt NPs, and the possible favorable properties of self-assembly might provide a bright venue for future magnetic recording media.

1. Introduction

FePt nanoparticles (NPs) have attracted a great deal of attention in the past decades because of their widespread applications in magnetic data storage, electrocatalysis and biomedical research, etc [1–5]. FePt NPs are well-known to have a chemically ordered face-centered tetragonal (fct) phase and a chemically disordered face-centered cubic (fcc) structure. Generally, the fct-FePt NPs are ferromagnetic and the derived arrays are considered as the prospective magnetic-media candidates [6,7], but the fcc-FePt NPs can exhibit superparamagnetic performances and demonstrate tremendous potential in biomedical applications owing to their stability in physiological conditions [8,9]. The typical strategy of solution phase synthesis of FePt NPs combining the reduction of $Pt(acac)_2$ and the decomposition of $Fe(CO)_5$ often provided the fcc-FePt NPs and then a post-annealing process at high temperature was required to accomplish the phase transformation from fcc to fct [10]. Since then, much effort was devoted to optimizing the synthetic methods by developing single-source precursors [11–13] or adopting one-step pyrolysis approach [14]. Such improvements continually promoted the developments of FePt NPs and other related nanomaterials such as FePd [15,16], CoPt [17,18], CoPd [19], CoFe [20] NPs, etc.

Patterning of the fct-FePt NPs is essential to develop their applications in magnetic recording media. Currently, there are two major approaches to accomplish the goals for further patterned devices [21], one is the direct self-assembly of FePt NPs [22], and the other is preparing ordered patterns from the processing of the precursors with a subsequent in-situ synthesis of FePt NPs, Generally, the common approach for patterning organometallic compounds often involved the lithographic patterning [23,24], self-assembly or other techniques [25–27]. On this basis, our group had been devoted ourselves to expanding the lithographic route for the mass production of ferromagnetic patterns, and the detailed study from solution-processable metallopolymers to hemiphasmidic small molecule precursors and the various processing means such as nanoimprint lithography further promoted the developments of patterned FePt NPs [1,28,29]. Besides, tridentate coplanar structures of platinum complexes with the functionality of ferrocene

* Corresponding author.
** Corresponding author.
E-mail addresses: zqyu@szu.edu.cn (Z.-Q. Yu), wai-yeung.wong@polyu.edu.hk (W.-Y. Wong).

https://doi.org/10.1016/j.jorganchem.2019.04.015
0022-328X/

were also investigated in our previous reports [14,28], in which the strong Pt···Pt interactions and π-π stacking played an important role in affecting the formation of FePt NPs. Considering the supramolecular interactions in square-planar Pt(II) terpyridine complexes and the self-assembly performance of amphiphic block polymers, amphiphilic cationic Pt(II) terpyridyl complex with a ferrocene unit could be easily assembled into vesicles [30], which suggests that the amphiphilic design could endow the materials with excellent properties of self-assembly due to the huge differences in the molecular structures. Hence, the amphiphilic blocks could be substituted by the corresponding hydrophobic groups and another different hydrophilic units, and then the amphiphilic properties would be accomplished.

Herein, two amphiphilic Fe,Pt-containing polymers **P1** and **P2** with different chain length of the tail unit were synthesized and fully characterized, where the ferrocene-modified Pt(II) terpyridyl complex and different length of the poly(ethylene glycol) (PEG) tail together formed the two blocks. The polymers acted as the single-source precursors to prepare ferromagnetic fct-FePt NPs by a one-step pyrolysis, and the resultant FePt NPs identified the effect of structural aggregation and intramolecular variation on their size and magnetic properties.

2. Experimental section

2.1. General

All reactions were carried out under nitrogen unless otherwise stated. Commercially available reagents were used as received without further purification. S1 [31] and $(DMSO)_2PtCl_2$ [14] were synthesized and purified according to the literature procedures. All reactions were monitored by thin-layer chromatography (TLC) with Merck pre-coated glass plates, and the compounds were visualized with UV light irradiation at 254 nm. Purification of products was achieved by column chromatography (silica gel or neutral aluminium oxide). NMR spectra were measured in $CDCl_3$ on a Bruker AV 400 NMR instrument with chemical shifts being referenced against tetramethylsilane as the internal standard for ^1H and ^{13}C NMR data. The thermogravimetric analysis (TGA) was performed with a Perkin Elmer TGA 6 thermal analyser.

The structural characterization of the as-synthesized FePt NPs was performed by powder X-ray diffraction (XRD) on a Bruker D8 machine with Cu $K_{\alpha1}$ ($\lambda = 540$ nm, 40 kV, 30 mA) for analyzing the composition and phase purity of the resulting FePt NPs. Transmission electron microscopy (TEM) and energy dispersive spectroscopy (EDX) analysis were carried out on a Philips Tecnai G2 20 S-TWIN for probing the morphology, lattice fringe, particle size and atomic ratio of Fe and Pt. The magnetic hysteresis loops at room temperature were measured by a quantum design physical property measurement system (PPMS).

2.2. Synthesis of amphiphilic bimetallic precursors

S2: 4-Hydroxybenzaldehyde (0.34 g, 2.8 mmol), monotosylated poly(ethylene glycol) **S1** (Mw = 550, 2.02 g, 3 mmol) and excess K_2CO_3 (1.16 g, 8.4 mmol) were dissolved in anhydrous N,N-dimethylformamide (40 mL). The mixture was magnetically stirred and heated at 70 °C for 24 h. The resultant solution was poured into water and extracted with dichloromethane. The dichloromethane solution was washed with water, dried over anhydrous sodium sulfate, and then filtered. The solvent was removed and the crude product was purified by column chromatography (silica gel) using CH_2Cl_2 to yield the compound **S2** (1.37 g, 79%). ^1H NMR ($CDCl_3$, 400 Hz, δ/ppm) 9.81 (s, 1H), 7.76 (d, $J = 8.8$ Hz, 2H), 6.96 (d, $J = 8.4$ Hz, 2H), 4.15 (t, $J = 4.8$ Hz, 2 H), 3.84–3.81 (m, 2H), 3.67–3.65 (m, 2H), 3.62–3.53 (m, 32 H), 3.49–3.47 (m, 2H), 3.31 (s, 3H).

S3: 2-Acetylpyridine (0.35 g, 2.86 mmol) and **S2** (1.1 g, 1.43 mmol) were dissolved in EtOH (50 mL), and KOH (0.32 g, 5.72 mmol) and aq. NH_3 (10 mL, 28%) were added to the solution, and then the mixture was stirred at 50 °C for 24 h. The mixture was then cooled to room temperature, the solvents was removed and the residue was extracted by CH_2Cl_2. The crude product was purified by a short column eluting by CH_2Cl_2 to give the target compound **S3** (1.01 g, 83%). ^1H NMR ($CDCl_3$, 400 Hz, δ/ppm) 8.69–8.65 (m, 6H), 8.05–8.02 (m, 2H), 7.89–7.80 (m, 4H), 7.48–7.45 (m, 2H), 4.20 (t, $J = 4.8$ Hz, 2 H), 3.91–3.88 (m, 2H), 3.75–3.73 (m, 2H), 3.70–3.60 (m, 32 H), 3.54–3.52 (m, 2H), 3.36 (s, 3H).

S4: $(DMSO)_2PtCl_2$ (171.4 mg, 0.2 mmol) and **S3** (84.5 mg, 0.2 mmol) were mixed in 15 mL of MeCN. The solution was refluxed overnight, and the solvent was removed *in vacuo* to give the product (222.3 mg, 95%). ^1H NMR (DMSO-d_6, 400 Hz, δ/ppm) 8.72–8.64 (m, 2H), 8.31 (s, 2H), 8.18 (s, 2H), 8.03 (s, 2H), 7.81 (s, 2H), 7.38 (s, 2H), 6.98 (d, $J = 8$ Hz, 2H), 4.19 (t, $J = 4.8$ Hz, 2 H), 3.87–3.85 (m, 2H), 3.72–3.69 (m, 2H), 3.61–3.54 (m, 32 H), 3.48–3.46 (m, 2H), 3.34 (s, 3H).

S5: To a solution of ferrocenylmethanol (1.62 g, 7.5 mmol) in dry THF (15 mL), NaH (0.45 g) was added slowly at 0 °C. After stirring for 0.5 h, 1-bromo-4-(bromomethyl)benzene (1.88 g, 7.5 mmol) in THF (10 mL) was added dropwise and the reaction mixture was stirred overnight at 60 °C. The reaction mixture was quenched with saturated aq. NH_4Cl (50 mL) at 0 °C and extracted with CH_2Cl_2. The organic extracts were washed with brine, dried over anhydrous Na_2SO_4 and concentrated under reduced pressure. The residue was purified by column chromatography to afford a yellow solid (2.25 g, 78%). ^1H NMR ($CDCl_3$, 400 Hz, δ/ppm) 7.47 (dt, $J_1 = 8.4$ Hz, $J_2 = 2$ Hz, 2H,), 7.21 (d, $J = 8.4$ Hz, 2H), 4.45 (s, 2H), 4.32 (s, 2H), 4.24 (t, $J = 1.6$ Hz, 2H), 4.17 (t, $J = 1.6$ Hz, 2H), 4.12 (s, 5H); ^{13}C NMR ($CDCl_3$, 100 Hz, δ/ppm) 137.6, 131.4, 129.3, 121.3, 83.1, 70.8, 69.4, 68.6, 68.5, 68.4.

S6: To the solution of **S5** (0.97 g, 2.5 mmol) in triethylamine (25 mL) and dichloromethane (25 mL) was added $Pd(PPh_3)_4$ (150 mg) and CuI (50 mg). After the solution was stirred for 30 min at 0 °C, trimethylsilylacetylene (1.5 ml) was then added and the suspension was stirred for 30 min. The mixture was subsequently heated to 75 °C for 24 h. The solution was concentrated and the residue was purified by column chromatography. The obtained intermediate was then dissolved in MeOH/CH_2Cl_2 (30 mL, v/v = 1/1), excess K_2CO_3 (0.69 g, 5 mmol) was added, and the mixture was stirred overnight. The product **S6** was obtained by extracting the reaction mixture with CH_2Cl_2 in a quantitative yield. IR (KBr, cm^{-1}): 2108 (C≡C), 3271 (C≡C-H stretching); ^1H NMR ($CDCl_3$, 400 Hz, δ/ppm) 7.47 (d, $J = 8$ Hz, 2H), 7.29 (d, $J = 8.4$ Hz, 2H), 4.50 (s, 2H), 4.32 (s, 2H), 4.24 (t, $J = 2$ Hz, 2H), 4.16 (t, $J = 1.6$ Hz, 2H), 4.12 (s, 5H), 3.07 (s, 1H).

P1: To a mixture of **S4** (0.38 g, 0.34 mmol) and **S6** (0.11 g 0.34 mmol) in CH_3Cl/*i*-Pr_2NH (v/v = 1/1) was added CuI (1 mg). The solution was stirred for 24 h at 40 °C. The solvent was removed under vacuum and the residue was filtered through a short alumina column to give the amphiphilic polymer **P1**. ^1H NMR ($CDCl_3$, 400 Hz, δ/ppm) 9.01–8.99 (m, 4H), 8.84–8.74 (m, 2H), 8.18 (s, 4H), 7.43–7.40 (m, 4H),7.30 (s, 2H), 6.89 (s, 2H), 4.52 (s, 2H), 4.38 (s, 2H), 4.29 (s, 2H), 4.19 (s, 5H), 4.14 (s, 4 H), 3.87 (s, 2H), 3.73–3.68 (m, 2H), 3.61–3.54 (m, 32 H), 3.48–3.46 (m, 2H), 3.34 (s, 3H).

P2: The polymer **P2** was prepared according to the similar

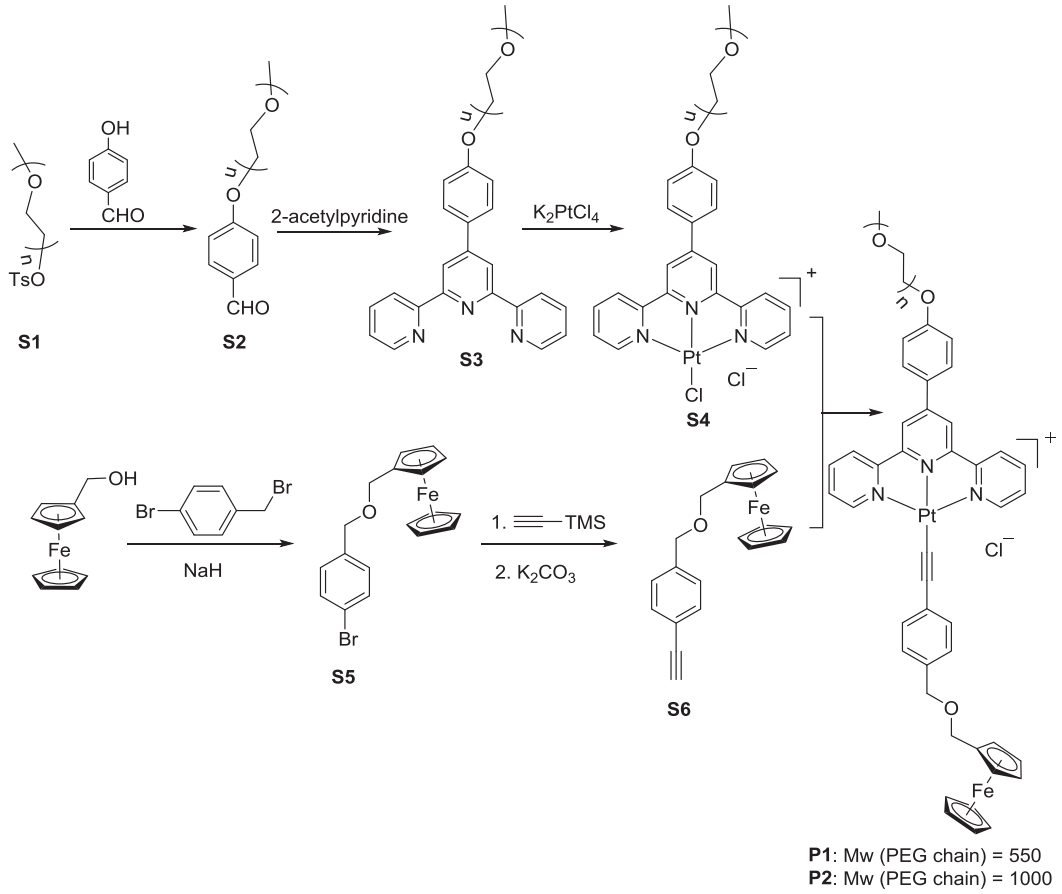

Scheme 1. Synthetic routes of the amphiphilic Fe,Pt-containing bimetallic polymers.

synthetic routes as **P1**, but the PEG with the M_w of 1000 was used instead.

2.3. Preparation of FePt nanoparticles

The polymer **P1** or **P2** was put in a ceramic boat first, and then it was placed in a tube furnace equipped with temperature and gas-flow controls. The precursor was heated for 1 h under an Ar/H_2 atmosphere at 800 °C. After cooling to room temperature, black powdery FePt NPs were formed. The resultant NPs pyrolyzed from **P1** and **P2** were named as **FePt-1** and **FePt-2**, respectively.

3. Results and discussion

The amphiphilic polymers **P1** and **P2** were designed and synthesized, in which the hydrophilic tail of poly(ethylene glycol) with different molecular weight of 550 and 1000 was used in **P1** and **P2**, respectively; the other hydrophobic tail was linked by a terpyridine ligand, and then the ligand was further coordinated to platinum by reacting the functional bond of Pt-Cl with a terminal alkyne-anchored Fe-containing compound to give the bimetallic sources with equal atomic ratio. Analysis of the TGA trace for the polymers indicated the good thermal stability with a high onset decomposition temperature of 331 °C. Here, all the Fe,Pt-containing groups acted as the hydrophobic blocks in the amphiphilic polymers. The amphiphilic compounds were used as the single-source precursors to prepare $L1_0$-FePt NPs by one-pot pyrolysis at 800 °C for 1 h under an Ar/H_2 (v/v = 95/5) atmosphere, and the resultant FePt NPs were named as **FePt-1** and **FePt-2** according to their respective precursors of **P1** and **P2**.

The morphology and lattice fringes of FePt NPs were identified by TEM and high-resolution TEM measurements. The corresponding images of **FePt-1** and **FePt-2** are shown in Figs. 1a and 2a, respectively. Both of them had a spherical shape with a very narrow size distribution and the generated NPs were evenly embedded in amorphous carbon matrix, but the mean size dimension presented a big difference. As statistically analyzed from the TEM image in a wide area, **FePt-1** and **FePt-2** had an average size of 24.7 nm (Figs. 1b) and 8.2 nm (Fig. 2b), respectively. Besides, high-resolution TEM image further indicated the high crystallinity of the resultant FePt NPs. The measured lattice fringes of 0.283 and 0.384 nm (Fig. 1c) of the individual single-crystal NPs are consistent with the *d*-spacing known for the (111) and (001) planes of the fct FePt NPs. Similarly, the lattice fringe of 0.221 nm (Fig. 2c) corresponding to the (110) plane was also observed in **FePt-2** NPs. The crystal structure from high-resolution TEM image revealed that the resultant **FePt-1** and **FePt-2** NPs possessed a chemically ordered fct structure.

FePt NPs with fct phase usually exhibit ferromagnetic performance, and the magnetic behavior was characterized here to deeply investigate the resultant FePt NPs. The magnetic hysteresis loop at room temperature was obtained by PPMS for **FePt-1** (Fig. 1d) and **FePt-2** (Fig. 2d), respectively. The hysteresis loops

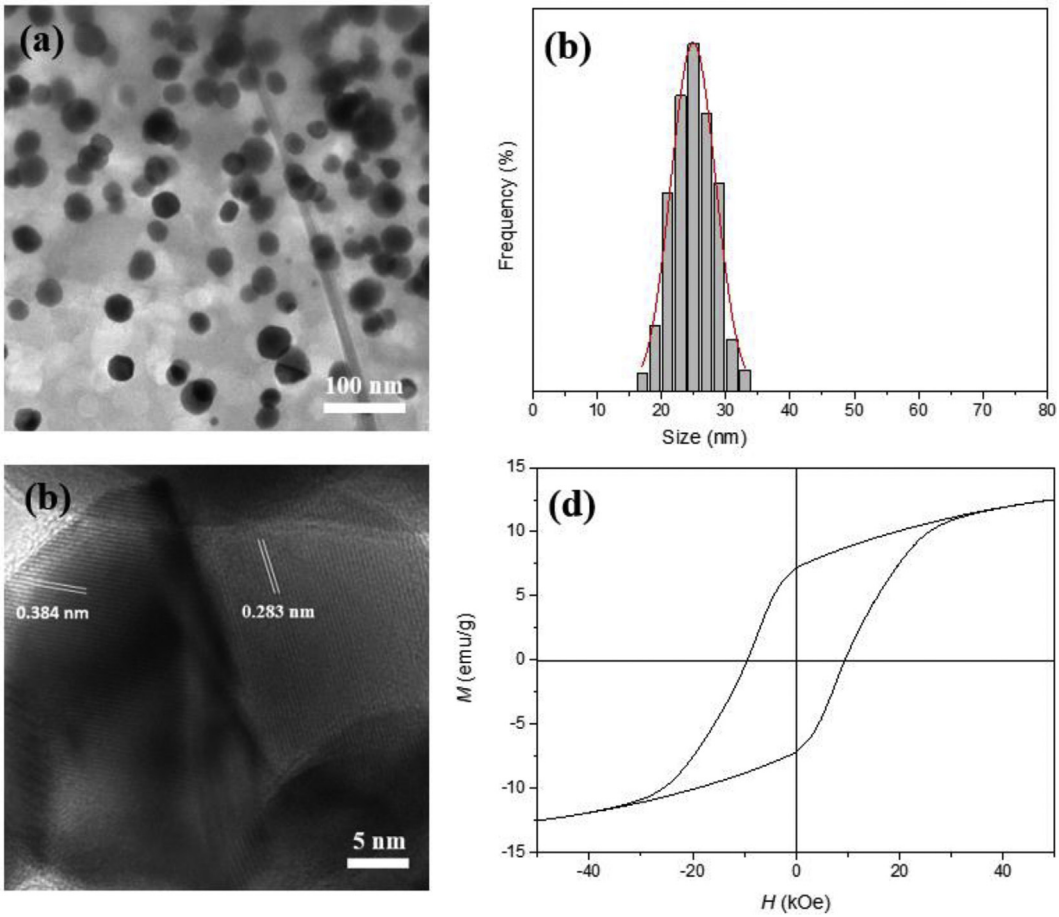

Fig. 1. The as-synthesized **FePt-1** NPs pyrolyzed from **P1**: (a) TEM image, (b) size distribution histogram statistically analyzed from the TEM image, (c) high resolution TEM image with lattice fringes, (d) room temperature hysteresis loop.

indicated that the resultant FePt NPs were ferromagnetic, the respective coercivity of **FePt-1** and **FePt-2** was 9.6 and 1.3 kOe, and the saturated magnetic moments were also measured as 12.5 emu·g^{-1} for **FePt-1** and 6.1 emu·g^{-1} for **FePt-2**. The big difference in coercivity might be due to the fact that **FePt-1** had a higher crystallinity than **FePt-2**, which was consistent with the XRD analysis; the discrepancy in magnetic moment could be ascribed to the different mass of PEG chain from the bimetallic precursors.

Powder XRD was also measured to identify the composition and phase of the as-synthesized FePt NPs. The observed XRD plots for **FePt-1** and **FePt-2** are shown and compared in Fig. 3. Well-resolved diffraction peaks of (001), (110), (111), (200), (201), (112) and (200) were indexed to the typical peaks of FePt (JCPDS card no. 043–1359) alloys with a chemically ordered fct phase. The appearance of the peaks (001) and (110) indicated that the resultant NPs had a fct structure. In addition, the stronger intensity of (001) and the obvious splitting of (200)/(002) and (220)/(202) further demonstrated the high crystallinity. However, the degree of ordering in **FePt-1** was obviously higher than that in **FePt-2** according to the splitting of the (200)/(002) and (220)/(202) pairs of reflections, and the results could further support their big differences in coercivity. In addition, the mean size calculated by the Scherrer analysis from the full width at the half-maximum of the (111) peak also agreed with the previous results in the TEM images.

The most possible reasons that resulted in the differences for **FePt-1** and **FePt-2** NPs were the structural variation of their respective precursors. In short, the amphiphilic design in the precursors is good for the Fe,Pt-containing block to assemble together and form a PEG-tailed bimetallic aggregates, which would make the resultant FePt NPs to have a uniform morphology. There is also other intermolecular interaction in the polymers' aggregates apart from the intramolecular motion from the two different blocks. Square-planar Pt(II) terpyridine framework might further increase the supramolecular interactions by the possible Pt···Pt interaction and π-π conjugation. In addition, the length of the PEG tails could affect the size of the FePt NPs. Long tails would weaken the intermolecular interaction of the Fe,Pt-containing block, and further decrease the aggregation of the metallic cores. This is similar to the previous report for tuning the size of FePt or FePd NPs by controlling the metallic fractions in the polymer precursors [32,33].

4. Conclusions

In conclusion, a novel class of Fe,Pt-containing polymers with amphiphilic design was synthesized and used as the single-source precursors to directly prepare ferromagnetic FePt NPs with very

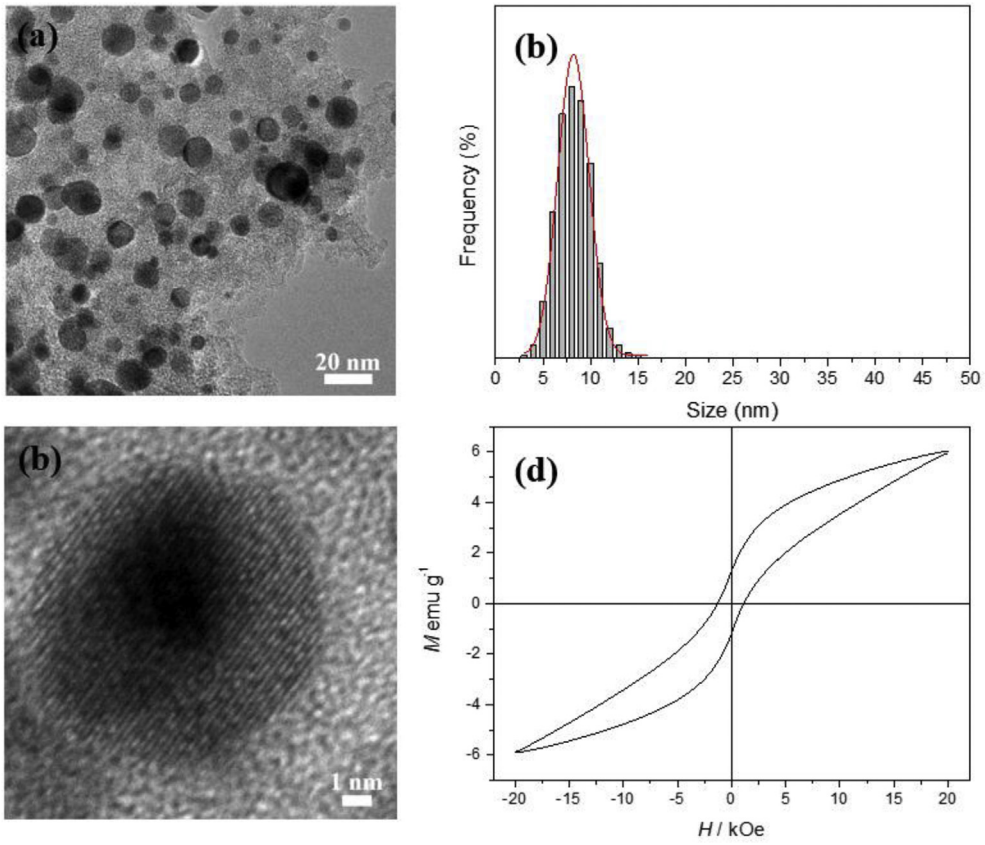

Fig. 2. The as-synthesized **FePt-2** NPs pyrolyzed from **P2**: (a) TEM image, (b) size distribution histogram statistically analyzed from the TEM image, (c) high-resolution TEM image with lattice fringes, (d) room temperature hysteresis loop.

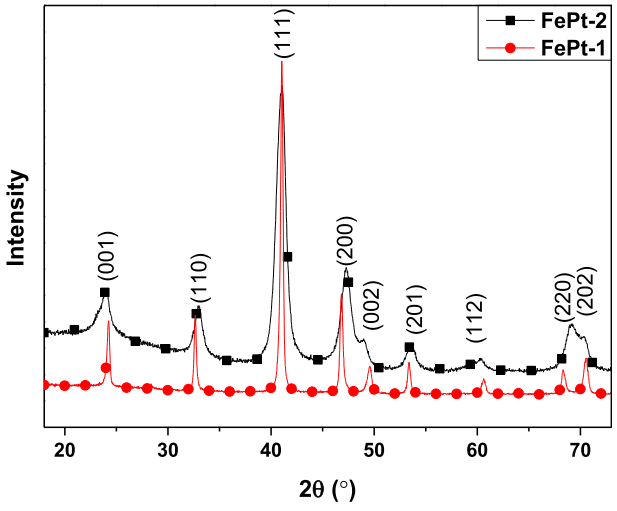

Fig. 3. Powder XRD patterns of the as-synthesized FePt NPs **FePt-1** and **FePt-2**.

high crystallinity. The PEG tails could act as the protective layer during pyrolysis, which would make the resultant NPs disperse more evenly in the carbon matrix; to some extent the size can also be controlled by tuning the length of the PEG tails. Self-assembly might be introduced in future application for developing magnetic recording media.

Acknowledgements

This work was supported by the National Natural Science Foundation of China (21701112, 51573151), Hong Kong Research Grants Council (PolyU153062/18P), the Hong Kong Polytechnic University (1-ZE1C) and Ms Clarea Au (847S) for the Endowed Professorship in Energy. Special thanks were also given to Instrumental Analysis Center of Shenzhen University (Xili Campus).

Appendix A. Supplementary data

Supplementary data to this article can be found online at https://doi.org/10.1016/j.jorganchem.2019.04.015.

References

[1] Q.C. Dong, Z.G. Meng, C.L. Ho, H.E. Guo, W.Y. Yang, I. Manners, L.L. Xu, W.-Y. Wong, Chem. Soc. Rev. 47 (2018) 4934–4953.
[2] M.H. Shao, Q.W. Chang, J.P. Dodelet, R. Chenitz, Chem. Rev. 116 (2016) 3594–3657.
[3] K. Zhu, Y.M. Ju, J.J. Xu, Z.Y. Yang, S. Gao, Y.L. Hou, Acc. Chem. Res. 51 (2018) 404–413.
[4] L.H. Wu, A. Mendoza-Garcia, Q. Li, S.H. Sun, Chem. Rev. 116 (2016) 10473–10512.
[5] S.H. Sun, Adv. Mater. 18 (2006) 393–403.
[6] Q. Dong, G.J. Li, C.L. Ho, M. Faisal, C.W. Leung, P.W.T. Pong, K. Liu, B.Z. Tang, I. Manners, W.-Y. Wong, Adv. Mater. 24 (2012) 1034–1040.
[7] Z.G. Meng, G.J. Li, H.F. Wong, S.M. Ng, S.C. Yiu, C.L. Ho, C.W. Leung, I. Manners, W.-Y. Wong, Nanoscale 9 (2017) 731–738.
[8] Y. Kitamoto, J.S. He, Electrochim. Acta 54 (2009) 5969–5972.
[9] P.C. Chiang, D.S. Hung, J.W. Wang, C.S. Ho, Y.D. Yao, IEEE Trans. Magn. 43 (2007) 2445–2447.

[10] S.H. Sun, C.B. Murray, D. Weller, L. Folks, A. Moser, Science 287 (2000) 1989–1992.
[11] R.D. Rutledge, W.H. Morris 3rd, M.S. Wellons, Z. Gai, J. Shen, J. Bentley, J.E. Wittig, C.M. Lukehart, J. Am. Chem. Soc. 128 (2006) 14210–14211.
[12] A. Capobianchi, M. Colapietro, D. Fiorani, S. Foglia, P. Imperatori, S. Laureti, E. Palange, Chem. Mater. 21 (2009) 2007–2009.
[13] M.S. Wellons, W.H. Morris, Z. Gai, J. Shen, J. Bentley, J.E. Wittig, C.M. Lukehart, Chem. Mater. 19 (2007) 2483–2488.
[14] Z.G. Meng, G.J. Li, S.M. Ng, H.F. Wong, S.C. Yiu, C.L. Ho, C.W. Leung, W.-Y. Wong, Polym. Chem. 7 (2016) 4467–4475.
[15] Y.L. Hou, H. Kondoh, T. Kogure, T. Ohta, Chem. Mater. 16 (2004) 5149–5152.
[16] A.D. Russell, G.R. Whittell, M.F. Haddow, I. Manners, Organometallics 33 (2014) 5349–5357.
[17] T. Gong, Z.X. Gao, W.L. Bian, F.F. Tai, W.Q. Liang, W.T. Liang, Q.C. Dong, C. Dong, J. Organomet. Chem. 819 (2016) 237–241.
[18] Q.C. Dong, W.S. Qu, W.Q. Liang, K.P. Guo, H.B. Xue, Y.Y. Guo, Z.G. Meng, C.L. Ho, C.W. Leung, W.-Y. Wong, Nanoscale 8 (2016) 7068–7074.
[19] A. Zadesenets, E. Filatov, P. Plyusnin, I. Baidina, V. Dalezky, Y. Shubin, S. Korenev, A. Bogomyakov, Polyhedron 30 (2011) 1305–1312.
[20] Z.G. Meng, C.L. Ho, G.J. Li, S.M. Ng, H.F. Wong, C.W. Leung, W.-Y. Wong, Mater. Res. Express 5 (2018), 115010.
[21] G.J. Li, C.W. Leung, Z.Q. Lei, K.W. Lin, P.T. Lai, P.W.T. Pong, Thin Solid Films 519 (2011) 8307–8311.
[22] R. Medwal, S. Gautam, S. Gupta, K.H. Chae, K. Asokan, G.R. Deen, R.S. Rawat, R.S. Katiyar, S. Annapoorni, IEEE Magn. Lett. 9 (2018), 5504105.
[23] K. Liu, C.L. Ho, S. Aouba, Y.Q. Zhao, Z.H. Lu, S. Petrov, N. Coombs, P. Dube, H.E. Ruda, W.-Y. Wong, I. Manners, Angew. Chem. Int. Ed. 47 (2008) 1255–1259.
[24] K. Liu, S. Fournier-Bidoz, G.A. Ozin, I. Manners, Chem. Mater. 21 (2009) 1781–1783.
[25] Y. Ma, P.F. She, K.Y. Zhang, H.R. Yang, Y.Y. Qin, Z.H. Xu, S.J. Liu, Q. Zhao, W. Huang, Nat. Commun. 9 (2018) 3.
[26] H.N. Al-Kharusi, L.P. Wu, G. Whittell, R. Harniman, I. Manners, Polym. Chem. 9 (2018) 2951–2963.
[27] G.J. Li, Z.G. Meng, J.S. Qian, C.L. Ho, S.P. Lau, W.-Y. Wong, F. Yan, Mater. Today Energy 12 (2019) 155–160.
[28] Z.G. Meng, C.L. Ho, H.F. Wong, Z.Q. Yu, N.Y. Zhu, G.J. Li, C.W. Leung, W.-Y. Wong, Sci. China Mater. 62 (2019) 566–576.
[29] Q.C. Dong, G.J. Li, C.L. Ho, C.W. Leung, P.W.T. Pong, I. Manners, W.-Y. Wong, Adv. Funct. Mater. 24 (2014) 857–862.
[30] L.B. Xing, S. Yu, X.J. Wang, G.X. Wang, B. Chen, L.P. Zhang, C.H. Tung, L.Z. Wu, Chem. Commun. 48 (2012) 10886–10888.
[31] E. Lee, Z. Huang, J.H. Ryu, M. Lee, Chem. Eur J. 14 (2008) 6957–6966.
[32] E. Kang, H. Jung, J.G. Park, S. Kwon, J. Shim, H. Sai, U. Wiesner, J.K. Kim, J. Lee, ACS Nano 5 (2011) 1018–1025.
[33] Z.G. Meng, G.J. Li, N.Y. Zhu, C.L. Ho, C.W. Leung, W.-Y. Wong, J. Organomet. Chem. 849–850 (2017) 10–16.